New Journal of Physics
The open access journal at the forefront of physics

PAPER • OPEN ACCESS

Magneto-excitons in Cu_2O: theoretical model from weak to high magnetic fields

To cite this article: Sylwia Zielińska-Raczyńska *et al* 2019 *New J. Phys.* **21** 103012

New Journal of Physics
The open access journal at the forefront of physics

Deutsche Physikalische Gesellschaft DPG
IOP Institute of Physics

Published in partnership with: Deutsche Physikalische Gesellschaft and the Institute of Physics

OPEN ACCESS

RECEIVED
14 May 2019

REVISED
1 September 2019

ACCEPTED FOR PUBLICATION
19 September 2019

PUBLISHED
7 October 2019

PAPER

Magneto-excitons in Cu_2O: theoretical model from weak to high magnetic fields

Sylwia Zielińska-Raczyńska[1], Dmitry A Fishman[2], Clément Faugeras[3], Marek M P Potemski[3], Paul H M van Loosdrecht[4], Karol Karpiński[1], Gerard Czajkowski[1] and David Ziemkiewicz[1]

[1] Institute of Mathematics and Physics, UTP University of Science and Technology, Al. Prof. S. Kaliskiego 7, 85-789 Bydgoszcz, Poland
[2] Department of Chemistry, University of California, Irvine, CA 92697, United States of America
[3] Laboratoire National des Champs Magnétiques Intenses, CNRS-UGA-UPS-INSA-EMFL, F-38042, Grenoble, France
[4] Physics Institute II, University of Cologne, Köln, D-50937, Germany

E-mail: david.ziemkiewicz@utp.edu.pl

Keywords: Rydberg excitons, magneto-absorption, real density matrix

Abstract

Recent experimental and theoretical work on hydrogen-like absorption spectra of excitons in external magnetic fields revealed new effects when the Coulomb interaction becomes comparable to the magnetic perturbation. We present a theoretical approach that allows for calculation of absorption spectra for any value of magnetic field. This approach opens the possibility to compute the optical functions i.e. reflectivity, transmission and absorption including the excitonic effects for various strength of external magnetic field.

1. Introduction

The discovery of hydrogen-like absorption series of excitons, i.e. Rydberg excitons (RE) in cuprous oxide, Cu_2O, opened a new chapter in semiconductor physics [1].

Extraordinary properties of RE attracted an increasing attention during the last few years, specifically for excitons in high external magnetic fields ([2–6] and references therein). This model system is well-recognized as a convenient analog to a hydrogen atom, in which the high field' physics occurs already at moderate field strengths achievable in a laboratory. In contrast, for hydrogen atoms the high field limit occurs for conditions met near for instance white-dwarf stars [7, 8]. Recent observations of REs in Cu_2O demonstrated that the energy of the RE states display a complex splitting, crossing and anti-crossing behavior, even for low quantum numbers [3].

Based on the ratio of the exciton binding energy and the magnetic field energy, the RE system can be classified into three distinctive regions: weak, intermediate, and high field regimes. In the weak field regime the electron–hole Coulomb interaction dominates over the external field energy. This is the purely excitonic regime where the external magnetic field can be treated as a perturbation. The reverse is true for the high field regime. Here the physics is dominated by the Landau quantization of the individual electrons and holes, while the Coulomb interaction can be treated as perturbation. In between these extremes there is the interesting case of the intermediate regime where neither Coulomb nor external field energies dominate the physics. For this case, excitonic binding energies are comparable with the cyclotron energy (with the reduced electron–hole mass for excitons). The distinct regions can be quantified through the normalized field strength parameter $\gamma = B/B_{\mathrm{cr}}$, where B is the magnetic field strength, and $B_{\mathrm{cr}} = \hbar/e(a^*)^2$ is the critical magnetic field for a given exciton with Bohr radius a^*. In the case of lower excitons in Cu_2O ($n = 1, 2, 3$), the specific inherent properties of this medium play an important role, i.e. a small excitonic Bohr radius (about 1 nm) and large excitonic Rydberg energy give the critical field strength $B_{\mathrm{cr}} \sim 700$ T.

Each magnetic field regime requires a different theoretical approach, since a general solution of the corresponding Schrödinger equation is not known. For a very small $\gamma \sim 10^{-2}$, i.e. for weak fields, the magneto-optical properties of a semiconductor can be obtained by solving the corresponding Schrödinger equation perturbatively in the basis of unperturbed hydrogen eigenfunctions. In the opposite case of high fields, the quasi

particles (electrons and holes) move in an effective potential obtained by integrating over the fast movement in the magnetic field, and thus theoretically the problem is reduced to the solution of a one dimensional Schrödinger equation [9, 10]. The case of intermediate fields, for which $\gamma \sim 10^{-1}$, is more complicated and several methods have been proposed [11].

Pioneering experimental and theoretical investigations of excitons in Cu_2O in a magnetic field have been reported by Kobayashi *et al* [12]. These authors discussed spectra of the yellow exciton series for low main quantum number ($n = 2, 3, l = 1$) in magnetic fields up to 150 T. Theoretical studies [3, 4] using group theoretical approaches have discussed spectra of magnetoexcitons up to $n = 5$. It has been concluded that the region of high magnetic fields for excitons in Cu_2O can be reached within several Teslas from experiments performed up to 4 T [3]. In work by Artyukin *et al* [13], the experimental observations in magnetic field up to 32 T are presented and values for weak and intermediate regimes are discussed. Note, the limit between the intermediate and high fields is not sharply defined thus a smooth transition can be expected. While the theoretical method offering the uniform treatment of excitonic spectra in GaN for the whole range of magnetic fields, taking into account valence band mixing due to the quantum well confinement, has been presented in [14] and the paper [15] described the magnetoexciton spectrum of the wurtzite-type GaN in high magnetic field for various polarizations of light, we have developed the uniform treatment applicable not only to the low excitonc states, but also to RE. Our current and previous work utilizes an analytical approach based on the Real Density Matrix Approach (RDMA), also taking into account polaritonic effects. We demonstrated [6] that the RDMA method allows one to obtain analytical expressions for magneto-optical functions for any main quantum number within the Rydberg series. Here we discuss experimental (up to 32 T) and theoretical (up to 150 T) studies on the absorption of a Cu_2O crystal in the Faraday configuration ($\mathbf{B}\|\mathbf{k}\|z$). In contrast to previous work, all three field regimes are treated on an equal level, and solutions are offered allowing expressing the susceptibility of the system and its corresponding magneto-optical spectra. Our results are partially extended giving up the center-of-mass approach due to larger sample dimensions [6]—the reflected light inside the medium is no longer coherent and therefore polaritonic effect are not essential. In the case of intermediate field we fully account both for the Coulomb interaction and for the magnetic field, while for high magnetic fields the influence of Coulomb attraction will be considered only in the field direction.

The paper is organized as follows. In section 2 we present the description of the experimental setup for absorption measurements in Cu_2O in static magnetic fields up to 32 T. In the section 3 we recall the basic assumptions of the RDMA and resulting calculational scheme. The results from section 3 are then applied to the regime of weak fields (section 4), intermediate fields (section 5) and high fields (section 6). Conclusions are presented in section 7.

2. Experiment

The experimental setup is the same as that used and described in [13]. In short, the magneto-absorption experiments were performed in Faraday geometry, at magnetic fields up to 32 T generated by a resistive magnet at the Grenoble High Magnetic Field Laboratory. Single crystal of cuprous oxide of [100] orientation, grown by a floating zone technique has been used for experiments. The sample has been placed in bath cryostat cooled down to 1.2 K, which was inserted into a 32 T bitter magnet. The light from a halogen lamp source has been delivered to the sample and collected after transmission through optical fibers and a combination of sheet quarter wavelength plates mounted on the sample holder for both the input and transmitted beam. The transmitted light has been detected with a monochromator equipped with a liquid nitrogen cooled CCD detector with a resolution of 0.02 nm. The experimental results are presented in figures 1–3.

3. Theory

For the Faraday geometry experiment, we can compute the linear response of a semiconductor slab of thickness L to a plain electromagnetic wave, whose electric field vector has a component of the form

$$E_i(z, t) = E_{\text{in}} \exp(\mathrm{i}k_0 z - \mathrm{i}\omega t), \qquad k_0 = \frac{\omega}{c}, \tag{1}$$

with the boundary surface of the semiconductor located at the plane $z = 0$. The second boundary is located at the plane $z = L$. In the case of the examined Cu_2O crystals the extension will be of the order 40 μm. Similar to our previous works, ([6] and references therein) we use RDMA. This method allows to obtain analytical expressions for magneto-optical functions of semiconductor crystals (reflectivity, transmissivity, absorption, and bulk susceptibility) for high main quantum numbers in the Rydberg series taking into account the coherence of the electron and hole with the radiation field. RDMA determines the positions of excitonic resonances in the

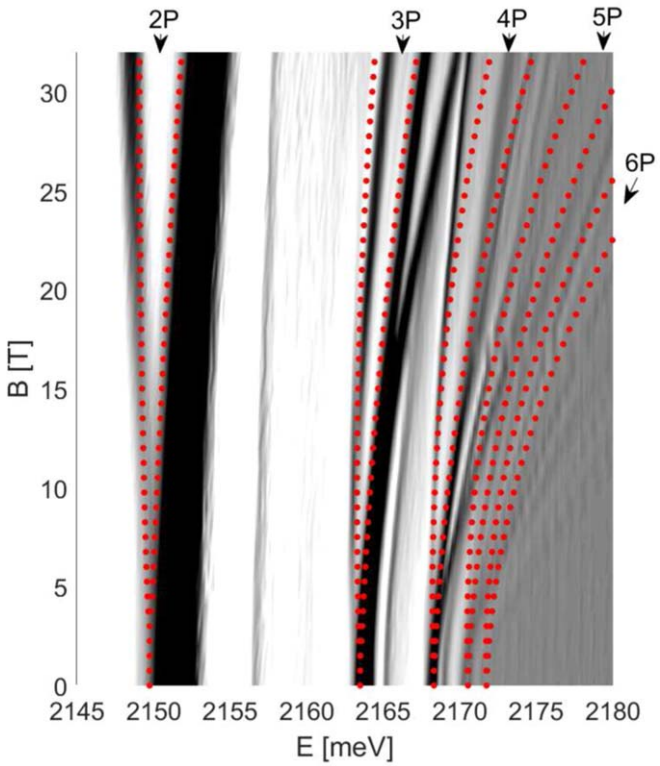

Figure 1. Positions of resonances calculated from the weak-field expansion (14), marked with red lines, compared with experimental data, for $B = 0$–32 T. The lines correspond to the yellow p excitons with $n = 2$–6. First derivative of susceptibility is used for clarity.

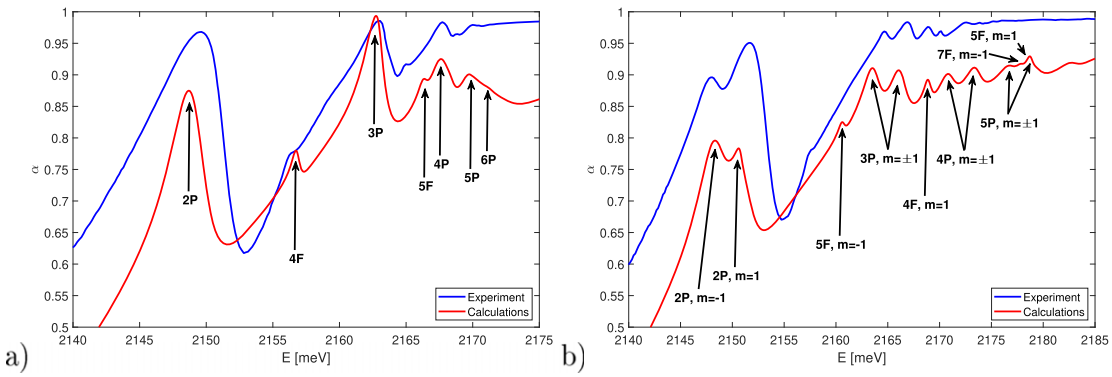

Figure 2. Comparison of measured and calculated absorption spectrum for (a) $B = 0$ and (b) $B = 32$ T.

situation when degeneracies of exciton states with different orbital and spin angular momentum are lifted by magnetic field. While only the weak field regime is considered in [6], we here extend the study into the intermediate and high magnetic field regimes. Within the RDMA approach, the relevant processes are described by a set of constitutive equations for the coherent amplitudes $Y^{\nu}(\mathbf{r}_e, \mathbf{r}_h)$ of the electron–hole pair of coordinates $\mathbf{r}_h$ (hole) and $\mathbf{r}_e$ (electron). In the case of Cu_2O ν means $p, f, h, \ldots$ excitonic states. The equations have been described in [2, 6] (see also [11, 16]) and have the form

$$\dot{Y}(\mathbf{R}, \mathbf{r}) + (\mathrm{i}/\hbar) H_{eh} Y(\mathbf{R}, \mathbf{r}) + (1/\hbar)\Gamma Y(\mathbf{R}, \mathbf{r}) = (\mathrm{i}/\hbar)\mathbf{M}(\mathbf{r})\mathbf{E}(\mathbf{R}), \tag{2}$$

where $\mathbf{R}$ is the excitonic center-of-mass coordinate, $\mathbf{r} = \mathbf{r}_e - \mathbf{r}_h$ is the relative coordinate, $\mathbf{M}(\mathbf{r})$ is the smeared-out transition dipole density, $\mathbf{E}(\mathbf{R})$ is the electric field vector of the wave propagating in the crystal, and operator Γ stands for the dissipative processes. We assume that this operator has the same eigenfunctions as the Hamiltonian H_{eh}, see also [17]. The dipole density $\mathbf{M}(\mathbf{r})$ is related to the bi-locality of the amplitude Y and

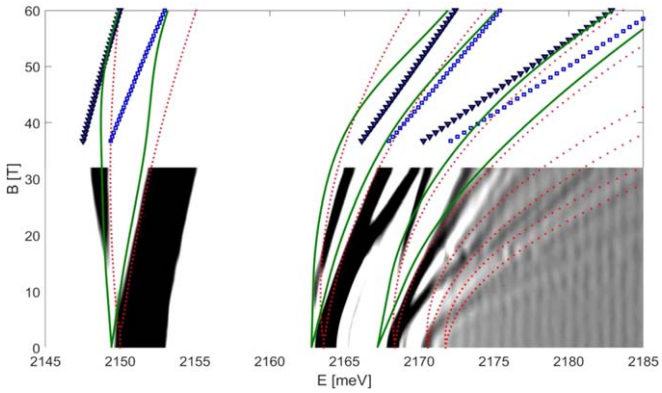

Figure 3. Calculated resonance positions in the regime of weak field (red dots) and intermediate field (blue dots). Green lines mark the total, joined solution for field range $B = 0$–64 T. Measured absorption is shown for $B \leqslant 32$ T.

describes the quantum coherence between the macroscopic electromagnetic field and the inter-band transitions. RDMA is a mesoscopic approach which, in the lowest order, neglects all effects from the multiband semiconductor structure, so that the exciton Hamiltonian becomes identical to that of the two-band effective mass Hamiltonian H_{eh}, which includes the electron and hole kinetic energy, the electron–hole interaction potential and the confinement potentials (see also [18]). When a constant magnetic field is applied, the Hamiltonian takes the form

$$H_{eh} = E_g + \frac{1}{2m_e}\left(\mathbf{p}_e + e\frac{\mathbf{B}\times\mathbf{r}_e}{2}\right)^2 + \frac{1}{2m_h}\left(\mathbf{p}_h - e\frac{\mathbf{B}\times\mathbf{r}_h}{2}\right)^2 - \frac{e^2}{4\pi\epsilon_0\epsilon_b|\mathbf{r}_e-\mathbf{r}_h|} + V_{\mathrm{conf}}(\mathbf{R},\mathbf{r}). \tag{3}$$

By separating the relative and center-of-mass coordinates and performing special unitary transformation (see, for example, [19, 20]), one can write the equation (3) in the form

$$H_{eh} = H_0 + \frac{\mathbf{P}^2}{2M_z} + \frac{p_z^2}{2\mu} + \frac{\mathbf{P}_\parallel^2}{2\mu} + \frac{1}{8}\mu\omega_c^2\rho^2 + \frac{e}{2\mu'}B\mathcal{L}_z - \frac{e}{M}\mathbf{P}_\parallel\cdot(r_\parallel\times\mathbf{B}) + V_{\mathrm{conf}}(\mathbf{R},\mathbf{r}), \tag{4}$$

where $\mathbf{P}$ is the exciton center-of-mass momentum operator, $\mathbf{P}_\parallel$ its in-plane component, the center-of-mass coordinates $\mathbf{R}_\parallel$ are separated from the relative coordinates (ρ, ϕ) on the plane (x, y), μ is the reduced mass for the electron–hole pair given by

$$\frac{1}{\mu} = \frac{1}{m_e} + \frac{1}{m_h}, \tag{5}$$

$\omega_c = eB/\mu$ is the cyclotron frequency, the reduced mass μ' defined as

$$\frac{1}{\mu'} = \frac{1}{m_e} - \frac{1}{m_h}, \tag{6}$$

and H_0 is the two-band Hamiltonian for the relative electron–hole motion,

$$H_0 = -\frac{\hbar^2}{2\mu}\nabla\underline{\underline{\mu}}\nabla - \frac{e^2}{4\pi\epsilon_0\epsilon_b|\mathbf{r}_e-r_h|}, \tag{7}$$

with the reduced mass tensor $\underline{\underline{\mu}}$. The operator $\mathcal{L}_z$ is the z-component of the angular momentum operator. We solve the constitutive equations with the above Hamiltonian to give the excitonic counterpart to the medium polarization

$$\mathbf{P}_{\mathrm{exc}}(\mathbf{R}) = 2\int \mathrm{d}^3r\ \mathbf{M}^*(\mathbf{r})\,Y(\mathbf{R},\mathbf{r}), \tag{8}$$

which is then used in the Maxwell field equation

$$c^2\nabla_R^2\mathbf{E} - \underline{\underline{\epsilon}}_b\ddot{\mathbf{E}}(\mathbf{R}) = \frac{1}{\epsilon_0}\ddot{\mathbf{P}}_{\mathrm{exc}}(\mathbf{R}), \tag{9}$$

with the use of the bulk dielectric tensor $\underline{\underline{\epsilon}}_b$ and the vacuum dielectric constant ϵ_0. In the current work we solve equations (2)–(9) and compute the magneto-optical functions (reflectivity, transmission, and absorption) for case of Cu_2O.

Below we will consider separately the cases of weak, intermediate and high magnetic fields.

Table 1. Band parameter values for Cu_2O, Rydberg energy and excitonic radius calculated from effective masses ($R^* = (\mu/\epsilon_b^2)13\,600$ meV, $a^* = (\epsilon_b/\mu)0.0529$ nm), masses in free electron mass m_0, critical field $B_{\rm cr} = \hbar/(e \times (a^*)^2)$.

Parameter	Value	Unit	Reference
E_g	2 172.08	meV	[1]
R^*	99.13	meV	
Δ_{LT}	1.25×10^{-3}	meV	[26]
Γ	0.8	meV	
m_e	1.0	m_0	[13]
m_h	0.7	m_0	[13]
μ	0.41	m_0	
μ'	−2.33	m_0	
a^*	0.97	nm	[13]
r_0	0.21	nm	[27]
ϵ_b	7.5		[1]
B_{cr}	700	T	

4. Weak magnetic fields

As we stated above, the dimensionless strength γ of the applied magnetic field, defines the regimes of weak, intermediate, and high fields. For weak fields $\gamma \ll 1$ which means that Coulomb interaction, thus excitonic states dominate the spectral properties and the magnetic field can be considered as a perturbation. Here we recall the basic equations from [6] where the weak field regime was discussed in the framework of RDMA. Due to the extension of the crystal in the direction of wave propagation, in contrast to [6] we will not account for the center-of-mass motion. Furthermore, to simplify the calculations, we assume the electron and hole masses to be isotropic. We consider the case of the Faraday configuration, with the magnetic field directed in the z-direction. We put $P_{\|} = 0$ in equation (4) and neglect the effects related to the center-of-mass motion and the confinement, so that the Hamiltonian takes the form

$$H_{eh} = H_0 + \frac{1}{8}\mu\omega_c^2\rho^2 + \frac{e}{2\mu'}B\mathcal{L}_z. \tag{10}$$

In the spirit of the perturbation calculus, we seek solution of the constitutive equation (2) in terms of eigenfunctions of the unperturbed Hamiltonian H_0

$$Y(\mathbf{r}) = \sum_{n\ell m} c_{n\ell m} R_{n\ell m}(r)\, Y_{\ell m}(\theta,\, \phi), \tag{11}$$

where $R_{n\ell}$ are the radial functions of a hydrogen-like Schrödinger equation

$$H_0\psi_{n\ell m} = E_{n\ell m}\psi_{n\ell m}, \tag{12}$$

where $\psi_{n\ell m} = R_{n\ell m}Y_{\ell m}$, with the spherical harmonics $Y_{\ell m}$, and the radial functions

$$R_{n\ell}(r) = \left(\frac{2}{na^*}\right)^{3/2} \frac{1}{(2\ell+1)!}\sqrt{\frac{(n+\ell)!}{2n(n-\ell-1)!}} \times \left(\frac{2}{na^*}\right)^{\ell} \mathrm{e}^{-r/na^*} M\left(-n+\ell+1,\, 2\ell+2,\, \frac{2r}{na^*}\right), \tag{13}$$

related to the eigenvalues $E_{n\ell}$ for p ($\ell = 1$) and f ($\ell = 3$) excitons, respectively [17]. The function $M(a, b, z)$ is the confluent hypergeometric function in the notation of Abramowitz [21], and R^* is the excitonic Rydberg energy. Inserting the expansion (11) into the constitutive equation (2) with the assumption of the harmonic time dependence, one obtains the following system of equations for the coefficients $c_{n\ell m}$

$$\sum_{n\ell m}\left(W_{n\ell m} + \frac{R^*}{4a^{*2}}\gamma^2 r^2 \sin^2\theta\right) \times c_{n\ell m}R_{n\ell}(r)\, Y_{\ell m}(\theta,\, \phi) = \mathbf{M}(\mathbf{r})\mathbf{E},$$
$$W_{n\ell m} = E_g - \hbar\omega + E_{n\ell} + \mathrm{sgn}(B)\, m\frac{\mu}{\mu'}\gamma R^* - \mathrm{i}\Gamma, \tag{14}$$

where a^* is the exciton Bohr radius, and $\gamma = \hbar\omega_c/2R^* = B/B_{\rm cr}$ is the dimensionless strength of the magnetic field. Using the shapes of the transition dipole density $\mathbf{M}$ appropriate for p and f excitons, and the band parameters for Cu_2O (table 1), we obtain the expansion coefficients and from that the function Y, which

defines the excitonic polarization by the equation (8). Since Y depends on the field (equation (2)), the equation (8) determines the functional dependence $\mathbf{P}_{\rm exc}(\mathbf{E})$ which, in the considered case, takes the form $\mathbf{P}_{\rm exc}(\mathbf{E}) = \epsilon_0 \chi \mathbf{E}$, χ being the susceptibility. Using χ, we can calculate the effective dielectric function, the effective refraction index, and from them, by standard formulae, the magneto-optical functions. In the calculations we used the eigenvalues $\Gamma_{n1\pm1}$ of the damping operator Γ (see (2)). Those values were estimated, for the case $B = 0$, by fitting the experimental absorption curves by Kazimierczuk *et al* [1], and Hecktötter *et al* [22], see also [23].

The results are illustrated in figures 1–2. Figure 1 depicts the calculated positions of excitonic resonances compared with our experimental data. The first derivative of the measured absorption, depicted in gray, is used for clarity. The red lines mark the peaks of the calculated absorption for P excitons with $n = 2$–6 and $m = \pm1$. They exhibit a good agreement with the measured data. A detailed view of the calculated susceptibility is shown in the figure 2. There is a close match between the resonance positions, both for $B = 0$ (figure 2(a)) and $B = 30$ T (figure 2(b)). Theoretical results were calculated for p and f excitons with quantum number $n = 2$–10, which allows us to identify the measured peaks. Important to note, there are multiple peaks assigned to f-excitons for $n \geqslant 4$. When the magnetic field is absent, the upper excitonic p states are located closely together around $E \approx Eg = 2174$ meV, while the f states converge to $E \approx 2172$ meV. When the magnetic field is applied, these levels are strongly blue-shifted, forming a complicated structure above the gap consisting of many crossing spectral lines, resulting from the Zeeman interaction.

5. Intermediate fields

For intermediate magnetic fields one has to include both Coulomb interaction and the influence of the magnetic field. This asks for a different theoretical approach, which may include (but is not limited to) variational or matrix diagonalization techniques[13]. In our studies we use a Green's function method [11]. First, we separate the 'kinetic+magnetic field' part H_{kin+B} and the electron–hole interaction term V of Hamiltonian

$$H_{kin+B}Y = \mathbf{M}\,\mathbf{E} - VY. \tag{15}$$

The following leads to the solution of (15) by means of an appropriate Green's function

$$Y = G\mathbf{M}\mathbf{E} - GVY. \tag{16}$$

It is important to note that 3 types of symmetry are accounted for in our work. Each case is characterized by an appropriate set of quantum numbers. In section 4 one deals with spherical symmetry of hydrogen-like atom with quantum numbers n, ℓ, m; $n = 1,\ldots,\ell = 0,\ 1,\ldots,m = 0,\ \pm1,\ldots$. The p states correspond to $m = 1$ and the lowest p state is given by $n = 2, \ell = 1, m = \pm1$. We here use the cylindrical symmetry and the discrete quantum numbers are $n_\rho = 0, 1, \ldots, m = 0,\ \pm\ 1, \ldots$. The lowest p state is given by $n_\rho = 1, m = \pm1$. Due to the properties of Cu_2O we start with $n_\rho = 1$. The Green's function in equation (16) satisfies, by definition, the equation

$$H_{\rm kin+B}G(\rho,\ \rho';\ z,\ z';\ \phi,\ \phi') = -\frac{\delta(\rho - \rho')}{2\pi\rho'}\delta(z - z')\delta(\phi - \phi'), \tag{17}$$

where the operator $H_{\rm kin+B}$ has the form

$$\begin{aligned} H_{\rm kin+B} &= H_1 + H_2, \\ H_1 &= \frac{p_\parallel^2}{2\mu} + \frac{e}{2\mu'}B\mathcal{L}_z + \frac{1}{8}\omega_c^2\rho^2, \\ p_\parallel^2 &= -\frac{1}{\rho}\frac{\partial}{\partial\rho}\frac{1}{\rho}\frac{\partial}{\partial\rho} - \frac{1}{\rho^2}\frac{\partial^2}{\partial\phi^2}, \\ H_2 &= \frac{p_z^2}{2\mu}, \quad p_z^2 = -\frac{\partial^2}{\partial z^2}, \end{aligned} \tag{18}$$

where we used cylindrical coordinates. The Green's function can be obtained by various methods (see, for example, [24] for details) where we have chosen the method of eigenfunctions expansion [11], taking the eigenfunctions $\psi_{n_\rho m}$ of the operator H_1

$$G(\rho,\ \rho';\ z,\ z';\ \phi,\ \phi') = \frac{1}{2\pi}\sum_{n_\rho,m}\psi_{n_\rho,m}(\rho)\psi_{n_\rho,m}(\rho')\exp[{\rm i}m(\phi - \phi')]g_{n_\rho m}(z,\ z'), \tag{19}$$

obtaining finally

$$G(\rho,\,\rho',\,\phi,\,\phi',\,\zeta,\,\zeta') = \frac{1}{2\pi}\sum_{n_\rho=1}^{\infty}\sum_{m=-n_\rho}^{n_\rho} \mathrm{e}^{\mathrm{i}m(\phi-\phi')} \times R_{n_\rho m}(\rho)R_{n_\rho m}(\rho')\frac{\exp[-k_{n_\rho m}|\zeta-\zeta'|]}{2k_{n_\rho m}},$$

$$R_{n_\rho m}(\rho) = \sqrt{\gamma}\sqrt{\frac{(n_\rho+|m|)!}{n_\rho!(m!)^2}} \times \left(\frac{\gamma\rho^2}{2}\right)^{|m|/2} \mathrm{e}^{-\gamma\rho^2/4} M\left(-n_\rho,\,|m|+1,\,\frac{\gamma\rho^2}{2}\right)$$

$$= \sqrt{\gamma}\sqrt{\frac{n_\rho!}{(n_\rho+|m|)!}}\left(\frac{\gamma\rho^2}{2}\right)^{|m|/2} \mathrm{e}^{-\gamma\rho^2/4} L_{n_\rho}^{|m|}\left(\frac{\gamma\rho^2}{2}\right), \tag{20}$$

where $n_\rho = 1,\ldots,|m| \leqslant n_\rho$, $M(a,b,z)$ is the confluent hypergeometric function, [21] L_n^m are Laguerre polynomials and

$$k_{n_\rho m}^2 = \frac{2\mu}{\hbar^2}a^{*2}(E_g - \hbar\omega - \mathrm{i}\Gamma) + U_{n_\rho m}/R^*,$$

$$U_{n_\rho m}/R^* = \gamma\left(2n_\rho + \mathrm{sgn}(B)\, m\frac{\mu}{\mu'} + |m| + 1\right). \tag{21}$$

In the above expressions we have used cylindrical variables scaled in the excitonic Bohr radii. The eigenfunctions $R_{n_\rho m}$ and eigen energies $U_{n_\rho m}$ are also termed Landau states and Landau energies. For the p excitons $n_\rho = 1$, $2,\ldots, m = \pm 1$ and the lowest Landau energies (including the Zeeman splitting) the energies are given by

$$U_{1,\pm1} = \left(\frac{B}{B_{\mathrm{cr}}}\right)\left(4 \pm \frac{\mu}{\mu'}\right)R^*, \tag{22}$$

while the exciton energy equals to R^*/n^2, thus the equation

$$\frac{B}{B_{\mathrm{cr}}} = \left[n^2\left(4 \pm \frac{\mu}{\mu'}\right)\right]^{-1} = \gamma_{\mathrm{cr}} \tag{23}$$

defines the limit of the weak field: $B < \gamma_{\mathrm{cr}}B_{\mathrm{cr}}$ for the weak field and $B \geqslant \gamma_{\mathrm{cr}}B_{\mathrm{cr}}$ for the intermediate field regime. As shown in the table 1, depending on the field orientation, the limiting values 45.71 and 49.3 T for $n = 2$ and around 21.9 T for $n = 3$ were obtained. The upper value corresponds to $B > 0$ and $m = -1$, and the lower to the quantum number $m = +1$ for the same field orientation.

The Green's function allows one to calculate the amplitude Y from the (16)

$$Y = \frac{2\mu}{\hbar^2 a^*}\mathcal{E}G\tilde{M} + G\frac{2}{\sqrt{\rho^2+\zeta^2}}Y, \tag{24}$$

where $\mathcal{E}$ is the amplitude of the propagating wave and $\tilde{M}$ the dipole density in scaled variables.

The detailed calculations follow the pattern presented for the electric field using the trial wave functions [2]. For p excitons the trial function has the form [11]

$$Y^{(P)} = R_{11}(\rho)\left[\sum_{m=\pm1} Y_{1m}^{(P)}\exp(-k_{1m}\sqrt{\rho^2+\zeta^2})\frac{\mathrm{e}^{\mathrm{i}m\phi}}{\sqrt{2\pi}}\right] + \sum_{n_\rho=2}^{\infty}\sum_{m=-n_\rho}^{n_\rho}\frac{\mathrm{e}^{\mathrm{i}m\phi}}{\sqrt{2\pi}}Y_{n_\rho m}^{(P)}(\zeta)R_{n_\rho m}(\rho), \tag{25}$$

with certain functions $Y_{nm}(\zeta)$. Furthermore, the y component of the dipole density of the form [2]

$$M_y^{(P)} = \sqrt{\frac{2}{\pi}}\frac{M_0}{\rho_0^3 a^{*3}} \times \rho\,\exp\left(-\frac{\rho^2}{2\rho_0^2}\right)\frac{\mathrm{e}^{\mathrm{i}\phi}+\mathrm{e}^{-\mathrm{i}\phi}}{\sqrt{2\pi}}\delta(\zeta), \tag{26}$$

with the given coherence radius $\rho_0 = r_0/a^*$. Since we consider a wave propagating through the crystal in the z-direction, which is linearly polarized in the plane (x, y), we can choose either x- or y-component of the field. We have chosen the y-component and, in correspondence, the M_y is the dipole density. The coherence radius r_0 is defined as [16, 25]

$$r_0^{-1} = \sqrt{\frac{2\mu\,E_g}{\hbar^2}}. \tag{27}$$

The integrated dipole strength M_0 and the coherence radius r_0 are connected through the longitudinal-transversal energy Δ_{LT} as [17]

$$M_0^2 = \frac{\hbar^2}{4\mu}\epsilon_0\epsilon_b a^* \frac{\pi\Delta_{\rm LT}}{R^*} f(r_0, a^*) \tag{28}$$

with

$$f(r_0, a^*) = \frac{\pi^2}{2}\left(\frac{a^*}{r_0}\right)^4\left(\frac{2r_0}{r_0 + 2a^*}\right)^6. \tag{29}$$

The longitudinal-transverse splitting, which is related with the exciton oscillator strength, describes the splitting between the transversal states (coupled with the light) and the longitudinal ones (decoupled from the light), can be estimated either experimentally, from the polariton dispersion curves, or theoretically, using other microscopic quantities as oscillator strength density. For the case of Cu_2O it has been calculated in [26] (see table 1), and this value is used in our calculations.

Knowing the coherence radius ($r_0 \approx 0.21$ nm) and the integrated dipole strength M_0, one can solve the Lippmann–Schwinger equation (16). Taking into account (8) and the dipole density (26) it is clear, that only the value $Y(\zeta = 0)$ contributes to the polarization. Substituting (25) into (24) and retaining the lowest expansion term in *GVY* one obtains the following expression

$$\begin{aligned} &R_{11}(\rho)\left[\sum_{m=\pm1} Y_{1m}^{(P)}\exp(-k_{1m}\rho)\frac{e^{im\phi}}{\sqrt{2\pi}}\right] + \sum_{n_\rho=2}^{\infty}\sum_{m=-n_\rho}^{n_\rho}\frac{e^{im\phi}}{\sqrt{2\pi}}Y_{n_\rho m}^{(P)}(0)R_{n_\rho m}(\rho) \\ &= \frac{2\mu}{\hbar^2 a^*}M_0\frac{e^{i\phi}}{\sqrt{2\pi}}\sum_{n_\rho=1}^{\infty}R_{n_\rho 1}(\rho)\frac{d_{n_\rho 1}^{(P)}}{k_{n_\rho,1}} + \frac{2\mu}{\hbar^2 a^*}M_0\frac{e^{-i\phi}}{\sqrt{2\pi}}\sum_{n_\rho=1}^{\infty}R_{n_\rho 1}(\rho)\frac{d_{n_\rho 1}^{(P)}}{k_{n_\rho,-1}} \\ &+ G(\rho, \rho'; \phi, \phi'; 0, \zeta')\frac{2}{\sqrt{\rho'^2 + \zeta'^2}} \times R_{11}(\rho')\left[\sum_{m=\pm1} Y_{1m}^{(P)}\exp(-k_{1m}\sqrt{\rho'^2 + \zeta'^2})\frac{e^{im\phi'}}{\sqrt{2\pi}}\right] \end{aligned} \tag{30}$$

where the last term in the above equation contains integration above the primed variables ρ', ζ', ϕ' , and

$$d_{n_\rho 1}^{(P)} = \sqrt{\frac{2}{\pi}}\frac{1}{\rho_0^3}\int_0^\infty \rho^2 d\rho\, R_{n_\rho 1}(\rho)\exp\left(-\frac{\rho^2}{2\rho_0^2}\right) = \frac{2}{\sqrt{\pi}}(\gamma\rho_0)\sqrt{n_\rho + 1}\frac{(1 - \gamma\rho_0^2/2)^{n_\rho}}{(1 + \gamma\rho_0^2/2)^{n_\rho+2}}. \tag{31}$$

We have calculated the amplitude Y (see appendix A), the polarization from (8), and, finally, the p-exciton contribution to the susceptibility which can be presented in the following form

$$\begin{aligned} \chi^{(P)} &= \frac{2}{\epsilon_0\mathcal{E}}\int d^3r M^{(P)}(\mathbf{r})Y^{(P)}(\mathbf{r}) = \epsilon_b\left(\frac{2\mu M_0^2}{\epsilon_0\epsilon_b\hbar^2 a^*}\right) \\ &\times\left\{\left[\sum_{m=\pm1}\langle R_{11}(\rho)|e^{-k_{1m}\rho - \rho^2/2\rho_0^2}\rangle\frac{[d_{11}^{(P)}]^2}{k_{1m}}\frac{1}{Q_m^{(P)}}\right] + \sum_{m=\pm1}\sum_{n_\rho=2}^{\infty}\frac{[d_{n_\rho 1}^{(P)}]^2}{k_{n_\rho m}}\right\}, \end{aligned} \tag{32}$$

where

$$\begin{aligned} &\langle R_{11}(\rho)|e^{-k\rho-\rho^2/2\rho_0^2}\rangle \\ &= \left[\frac{2\gamma\Gamma(4)}{2 + \gamma\rho_0^2}D_{-4}\left(k\sqrt{\frac{2}{2 + \gamma\rho_0^2}}\right) - \frac{\gamma^2\Gamma(6)}{(2 + \gamma\rho_0^2)^3}D_{-6}\left(k\sqrt{\frac{2}{2 + \gamma\rho_0^2}}\right)\right]\exp\left(\frac{k^2}{2(2 + \gamma\rho_0^2)}\right), \\ &Q_m^{(P)} = \langle (R_{11}^2(\rho)|e^{-k_{1m}\rho}\rangle - F^{(P)}(k_{1m}, \gamma), \\ &F^{(P)}(k_{1m}, \gamma) = \frac{4}{\pi}\int_0^\infty \frac{ds}{k_{11}^2 + s^2} \times \int_0^\infty \rho d\rho K_0(\rho\sqrt{k_{1m}^2 + s^2})[R_{11}(\rho)]^2, \\ &\langle R_{11}^2|e^{-k_{1\pm1}\rho}\rangle = \int_0^\infty \rho d\rho\, R_{11}^2(\rho)\, e^{-k_{1\pm1}\rho}, \end{aligned} \tag{33}$$

with $k = k_{1m}$ and $D_\nu(z)$ being the parabolic cylinder functions [27]. It can be proved that for $\gamma \to 0$, $Q_m^{(P)}$ takes the form

$$Q_m^{(P)} = \frac{\gamma^2}{k^9}\left[6k^4\left(k - \frac{1}{2}\right) - 30\gamma k^2\left(k - \frac{1}{3}\right) + 315\gamma^2\left(k - \frac{1}{4}\right)\right]. \tag{34}$$

Ultimately, by using the approximation (34), we obtain the resonance positions for the intermediate field regime. The results are shown on the figure 3. The intermediate field solutions are marked with light blue ($m = 1$) and dark blue ($m = -1$) dots. From these results it is clear that the lower limit of the intermediate regime is $B \approx 30$ T. For higher fields, the predicted energy shift is linear and is consistent with the low-field solution from 40 to 60 T. By using interpolation to link the solutions calculated for two regimes, one obtains the wide range solution marked by green lines. The two solutions are interpolated with the Gauss error function,

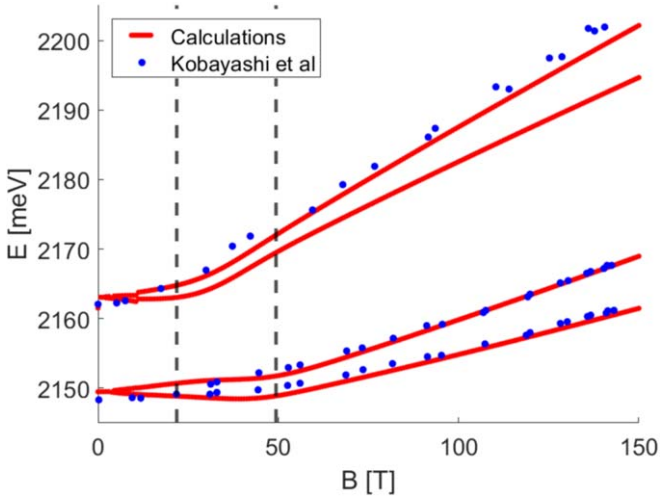

Figure 4. Calculated resonance positions compared with measured data by Kobayashi *et al* [12], in the range $B = 0$–150 T. Dashed lines mark the boundary between low- and intermediate field regime for $n = 2$ and $n = 3$.

where the transition value is $B = 40$ T for $n = 2$, 35 T for $n = 3$ and 30 T for $n = 4$. The linear dependence of energy on the magnetic field is in agreement with both our experimental results presented here is a close match to those obtained by Kobayashi *et al* [12] as shown on the figure 4. The calculated resonances show excellent agreement with experiments for $n = 2$ and $n = 3$ excitonic states. Again, note that transition to intermediate field regime is earlier for higher states. We have to remark that for these two regimes of magnetic field, we use two different methods of solution of the constitutive equation (2) and as the consequence one can not expect interpolation to be perfect. For the weak field we have used the perturbation calculus, where the unperturbed, spherically symmetric eigen-functions serve as a basis. For the intermediate fields equation (2) is transformed into an integral Lippmann–Schwinger equation, which is then solved with the help of an appropriate Green function and this problem has the cylindrical symmetry. As the integral equations can be solved in many ways we have used a certain trial function, which shape has a large impact on the accuracy of solutions. We have chosen the probe function given by equation (25), the form of which allows one to obtain solutions in an analytical form.

6. High magnetic fields

In the high fields limit the magnetic energy contributions to the Hamiltonian are much greater than the Coulomb term. The most simply definition of the high fields regime can be given in terms of the above introduced quantity γ, by the inequality $\gamma > 1$. When $\gamma > 1$, in the case of p-exciton, the lowest magnetic energy (Landau state) is larger than 4 Rydbergs, whereas the excitonic energies (absolute values) are smaller than $R^*/4$. So, the main optical effects in this regime, are the resonances at the above gap energies $E_g + U_{n_\rho m} R^*$, with $U_{n_\rho m}$ given by equation (21). But the Coulomb attraction cannot be neglected since, in spite of the action of the magnetic field, the average distance between the electron and hole decreases, and the Coulomb attraction increases. In consequence, one obtains a hydrogen-like series below every Landau state, as it was observed in the case of GaSe [28]. However, some comment is needed. As we show below, the satellite structures below the Landau states in GaSe are observed at a field strength with $\gamma < 1$, but satisfying the condition that the distance between the Landau states (about 4 R^* since GaSe has an indirect gap) is larger that $R^*/4$. If we consider the existence of hydrogen like series as the condition for the high field regime than, at least for GaSe, $\gamma = 0.1$ is the limiting value. Note that for higher values of γ, the visibility of the hydrogen series will be smaller, since the corresponding oscillator strengths will decrease with increasing γ, and the distances between the maxima in satellite structures decrease. As pointed by Aldrich *et al* [29], for GaSe at $\gamma = 4$ ($B_{cr} \sim 50$ T, $B \sim 200$ T), one observes the resonances at Landau energies, slightly red shifted for higher states, but the satellite structures were not observed. For Cu_2O, even for the fields as high as $B \sim 150$ T [12], one does not observe satellite structures in the vicinity of Landau states, typical for the high magnetic field regime. In this section we will present the analytical solution for Cu_2O, where we employ a one-dimensional polariton approximation. In this case the localization due to the magnetic field is stronger than that due to the Coulomb attraction, thus the effect of the latter is mainly in the field direction. One can say that the very rapid x–y motion is insensitive to the presence of the Coulomb field and that the slow z-component is determined by a potential which is the average of the Coulomb interaction over the rapid x–y motion. Please, note, that the approximation used for high magnetic

fields addresses 3 quantum numbers n_ρ, m, ℓ, with n_ρ starting from 1. Following this argument we assume for the coherent amplitude Y the form

$$Y(\rho,\,\zeta,\,\phi) = \sum_m \frac{1}{\sqrt{2\pi}} e^{im\phi} \sum_{n_\rho} R_{n_\rho m}(\rho)\, Y_{n_\rho m}(\zeta), \tag{35}$$

with unknown functions Y_{nm}. Using (35) with the constitutive equation (2), we obtain the following $z-$dependent parts of the amplitudes

$$\left(k^2_{n_\rho m} - \frac{\mathrm{d}^2}{\mathrm{d}\zeta^2} + V_{n_\rho m}(\zeta)\right) Y_{n_\rho m} = \frac{2\mu_\parallel}{\hbar^2 a^*} \langle \psi_{n_\rho m} | M \rangle\, \delta(\zeta), \tag{36}$$

with $k_{n_\rho m}$ defined in (21), and the effective Coulomb potentials $V_{n_\rho m}$

$$V_{n_\rho m}(\zeta) = -2 \int_0^\infty \rho \mathrm{d}\rho \frac{|R_{n_\rho m}|^2(\rho)}{\sqrt{\rho^2 + \zeta^2}}. \tag{37}$$

The adiabatic potentials $V_{n_\rho m}(z)$ are complicated expressions, which in previous treatments of the problem were solved numerically, or approximated by a simplified analytical approach [9]. For the sake of simplicity, we adopt here the expressions for the adiabatic potentials

$$V_{n_\rho m}(\zeta) = -\frac{2}{a_{n_\rho m} + |\zeta|} + \frac{A_{n_\rho m} a_{n_\rho m}}{[a_{n_\rho m} + |\zeta|]^2}, \tag{38}$$

with parameters $a_{n_\rho m}$, $A_{n_\rho m}$ chosen for each n_ρ, m to approximate $V_{n_\rho m}$ [9]. The one-dimensional Schrödinger equation (36), using the derived potentials, can be solved, with eigenfunctions $\varphi_{\ell n_\rho m}$ and eigenvalues $\varepsilon_{\ell n_\rho m}$,

$$\begin{aligned} \varepsilon_{\ell n_\rho m} &= -\left[\ell + \frac{1}{2} + \frac{1}{2}\sqrt{1 + 4\, A_{n_\rho m} a_{n_\rho m}}\right]^{-2}, \\ \varphi_{\ell n_\rho m}(t) &= N_{\ell s}\, t^{(s+1)/2} e^{-t/2} L^{(s)}_\ell(t), \\ N_{\ell s} &= \left[(2\ell + s + 1)\frac{\Gamma(s + \ell + 1)}{\ell!}\right]^{-1/2}, \end{aligned} \tag{39}$$

with Laguerre polynomials $L^{(s)}_\ell$, $\ell = 0,\, 1,\, 2,\ldots$, $t = 2\sqrt{-\varepsilon_{\ell n_\rho m}}(a_{n_\rho m} + |\zeta|)$, $s = \sqrt{1 + 4A_{n_\rho m} a_{n_\rho m}}$. Using these quantities, we obtain the amplitudes $Y_{n_\rho m}$ from (36), the polarization from (8) and finally the susceptibility

$$\chi \propto \sum_{P,F} \sum_{\ell n_\rho m} [d^{P,F}_{n_\rho m}]^2 \frac{\varphi^2_{\ell n_\rho m}(\zeta = 0)}{k^2_{n_\rho m} + \varepsilon_{\ell n_\rho m}}, \tag{40}$$

where

$$\begin{aligned} [d^{(F)}_{n_\rho m}]^2 &= \frac{64}{9\pi}(\gamma\rho_0)^2(n_\rho + 1), \quad m = \pm 1, \\ [d^{(F)}_{n_\rho m}]^2 &= \frac{16}{9\pi}(\gamma^2\rho_0^3)^2(n_\rho + 1)(n_\rho + 2)(n_\rho + 3), \quad m = \pm 3, \\ k^2_{n_\rho \pm 3} &= \frac{1}{R^*}(E_g - \hbar\omega - i\Gamma) + \gamma(2n_\rho \pm 3\frac{\mu}{\mu'} + 4). \end{aligned}$$

The total absorption, including p and f excitons, is given by

$$\chi = \chi^{(P)} + \chi^{(F)}, \tag{41}$$

with corresponding effective dielectric function $\epsilon = \epsilon_b + \chi^{(P)} + \chi^{(F)}$.

In appendix B, we present a detailed calculations based on equation (40). By certain assumptions on the coefficients $A_{n_\rho m}$, $a_{n_\rho m}$ we obtained an analytical expression for the susceptibility (40). The imaginary part of the susceptibility is displayed in figure 5, showing resonances below Landau energies. There are multiple, evenly spaced peaks above E_g, which shift towards higher energy with increasing B. The calculations were performed for Cu_2O data, but similar calculations can be done for GaSe data and the resulting line shape is very close to that observed experimentally by Mooser *et al* [28].

7. Conclusions

A theoretical solution to model absorption spectra due to excitons of Cu_2O in a wide range of external magnetic fields is presented. The approach differs from other approaches (matrix diagonalization, variational method etc) and uses the Green's function for the kinetic+magnetic part of the Hamiltonian combined with an appropriate trial function where Coulomb and magnetic interaction are accounted for. To our knowledge, this is the first

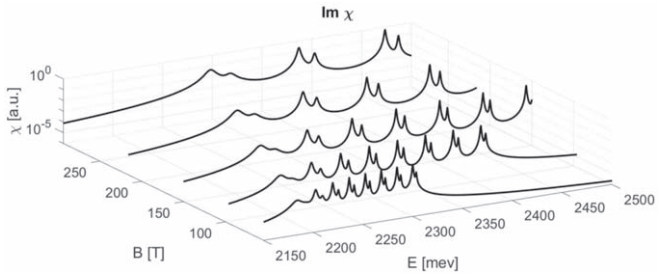

Figure 5. Imaginary part of susceptibility for $B = 50$–300 T and $n = 1.8$.

work, that offers such a complete approach, discussing the different regimes depending on the relative contribution of Coulomb interaction and external field perturbation. Introducing a field-dependent parameter γ allows us to estimate smooth boundaries between these ranges. Our results show good agreement with our experimental data measured in static field up to 32 T. In the intermediate range, up to $B = 150$ T, the results of our theoretical calculations show a good agreement with measurements by Kobayashi *et al* [12]. We have shown that for *p* excitons, the intermediate field regime start at a relatively small value of $\gamma \sim 0.06$, as opposed to *s* excitons.

Acknowledgments

Support from National Science Centre, Poland (project OPUS, CIREL 2017/25/B/ST3/00817) is greatly acknowledged.

Appendix A. Calculation of the amplitude Y

The last term on the rhs of (30) contains integration, so that (30) is an integral equation. From various methods of solving integral equations we choose the method of projection on a orthonormal basis $u_{nm}(\rho, \phi)$. We can use the functions $\psi_{nm} = R_{nm}(\rho)\exp(im\phi)/\sqrt{2\pi}$, to obtain

$$Y^{(P)}_{1\pm}\langle R^2_{11}, \mathrm{e}^{-k_{1\pm1}\rho}\rangle = \frac{2\mu}{\hbar^2 a^*}M_0\mathcal{E}\frac{d_{11}}{2k_{1\pm1}} + 2\sum_{m=\pm1} Y^{(P)}_{1m}\int \rho' \mathrm{d}\rho' \int \mathrm{d}\zeta' \left[\frac{\exp(-k_{1m}\sqrt{\rho'^2+\zeta'^2})}{\sqrt{\rho'^2+\zeta'^2}} \times \frac{\exp(-k_{1\pm1}|\zeta'|)}{2k_{1\pm1}} R_{11}(\rho')\right],$$

and from this the amplitudes

$$\begin{aligned}
Y_{1\pm1} &= \frac{2\mu}{\hbar^2 a^*}M_0\mathcal{E}\frac{d^{(P)}_{11}}{2k_{1\pm1}}\frac{1}{\langle R^2_{11}, \mathrm{e}^{-k_{1\pm1}\rho}\rangle - F^{(P)}(k_{1\pm1}, \gamma)},\\
\langle R^2_{11}, \mathrm{e}^{-k_{1\pm1}\rho}\rangle &= \int_0^\infty \rho \mathrm{d}\rho\, R^2_{11}(\rho)\, \mathrm{e}^{-k_{1\pm1}\rho},\\
Y^{(P)}_{n1}(0) &= \mathcal{E}\frac{2\mu}{\hbar^2 a^*}M_0\frac{d^{(P)}_{n1}}{2k_{n1}}, \quad n = 2, 3,\ldots,\\
Y_{n,-1}(0) &= \mathcal{E}\frac{2\mu}{\hbar^2 a^*}M_0\frac{d^{(P)}_{n1}}{2k_{n,-1}}, \quad n = 2, 3,\ldots\\
F^{(P)}(k_{1m}, \gamma) &= \frac{4}{\pi}\int_0^\infty \frac{ds}{k^2_{11}+s^2} \times \int_0^\infty \rho \mathrm{d}\rho K_0(\rho\sqrt{k^2_{1m}+s^2})[R_{11}(\rho)]^2.
\end{aligned} \tag{A.1}$$

Appendix B. Calculation of the susceptibility in high fields regime

Below we perform calculations for the high field regime where the satellite structures below the Landau states should appear. We use the expressions (40), taking only the *p* exciton contribution. The eigenfunctions have the form (39). To have an insight into the structure of solutions, we can simplify the problem by assuming $A_{n_\rho m} = 1$ and use the coefficients $a_{n_\rho m}$ in the form [10]

$$a_{n_\rho m} \rightarrow a_{\ell n_\rho m} = \sqrt{\frac{2n_\rho + \ell + 1}{\pi\gamma}}. \tag{B.1}$$

The choice of $A_{n_\rho m} = 1$ gives a good approximation to the adiabatic potentials obtained by numerical integration in equation (37), see also [30] As was observed in experiments by Mooser *et al* [28], the satellite structures below Landau energies occur at a small value of γ, for example $\gamma \approx 0.08$. Therefore the coefficients $a_{\ell n_\rho m}$ are large ($a_{\ell n_\rho m} \gg 1$) and following approximations can be made (we omit the indices):

$$\begin{aligned}
\sqrt{-\varepsilon} &= \frac{1}{(\ell + (1/2) + \sqrt{a})}, \\
t &= \frac{2}{\ell + (1/2) + \sqrt{a}}(a + \zeta), \\
s &= \sqrt{1 + 4A_{n_\rho m}a_{n_\rho m}} \approx 2\sqrt{a}, \\
t(0) &= 2a\frac{1}{\ell + (1/2) + \sqrt{a}} \\
[t(0)]^{(s+1)/2} &\approx \left(2a\frac{1}{\ell + (1/2) + \sqrt{a}}\right)^{\sqrt{a}+1/2}, \\
N_{\ell s} &= \left[(2\ell + s + 1)\frac{\Gamma(s + \ell + 1)}{\ell!}\right]^{-1/2} = \left[(2\ell + 2\sqrt{a} + 1)\frac{\Gamma(2\sqrt{a} + \ell + 1)}{\ell!}\right]^{-1/2}.
\end{aligned} \tag{B.2}$$

With the above assumptions and using the asymptotic expansion of the Gamma function $\Gamma(z)$ (for example, [21]) we have calculated the expressions $\Phi_{\ell n_\rho} = \ln[\varphi^2_{\ell n_\rho}(\zeta = 0)]$ (now $a_{\ell n_\rho}$ do not depend on the index m). Two examples are given below:

$$\begin{aligned}
\Phi_{0n_\rho} &= (2\sqrt{a_{0n_\rho}} + 1)\ln\left(\frac{2a_{0n_\rho}}{\sqrt{a_{0n_\rho}} + 1/2}\right) \\
&\quad - \left(2\sqrt{a_{0n_\rho}} + \frac{3}{2}\right)\ln(2\sqrt{a_{0n_\rho}} + 2) + (2\sqrt{a_{0n_\rho}} + 2) - \frac{2a_{0n_\rho}}{\sqrt{a_{0n_\rho}} + 1/2},
\end{aligned} \tag{B.3}$$

$$\begin{aligned}
\Phi_{1n_\rho} &= (2\sqrt{a_{1n_\rho}} + 1)\ln\left(\frac{2a_{1n_\rho}}{\frac{3}{2} + \sqrt{a_{1n_\rho}}}\right) - \ln(3 + 2\sqrt{a_{1n_\rho}}) \\
&\quad - \left(2\sqrt{a_{1n_\rho}} + \frac{3}{2}\right)\ln(2\sqrt{a_{1n_\rho}} + 2) + (2\sqrt{a_{1n_\rho}} + 2) - \frac{2a_{1n_\rho}}{\frac{3}{2} + \sqrt{a_{1n_\rho}}} \\
&\quad + 2\ln\left(1 + 2\sqrt{a_{1n_\rho}} - \frac{2\sqrt{a_{1n_\rho}}}{\frac{3}{2} + \sqrt{a_{1n_\rho}}}\right).
\end{aligned} \tag{B.4}$$

With the above assumptions, one can use the equation (40) to obtain the susceptibility.

ORCID iDs

Clément Faugeras https://orcid.org/0000-0002-9615-8739

References

[1] Kazimierczuk T, Fröhlich D, Scheel S, Stolz H and Bayer M 2014 *Nature* **514** 344
[2] Zielińska-Raczyńska S, Ziemkiewicz D and Czajkowski G 2018 *Phys. Rev.* B **97** 165205
[3] Schweiner F, Main J, Wunner G, Freitag M, Heckötter J, Uihlein C, Aßmann M, Fröhlich D and Bayer M 2017 *Phys. Rev.* B **95** 035202
[4] Schweiner F, Main J and Wunner G 2017 *Phys. Rev. Lett.* **118** 046401
[5] Fishman D 2008 Excitons in cuprous oxide *Thesis* University of Groningen
[6] Zielińska-Raczyńska S, Ziemkiewicz D and Czajkowski G 2017 *Phys. Rev.* B **95** 075204
[7] Isern J, García-Berro E, Külebi B and Lorén-Aguilar P 2017 *Astrophys. J. Lett.* **836** 2
[8] Kawka A 2018 The properties and origin of magnetic fields in white dwarfs. *Contrib. Astron. Obs. Skalnate Pleso* **48** 228–35
[9] Elliott E and Loudon R 1960 *J. Phys. Chem. Solids* **15** 196
[10] Ruf T, Phillips R, Cantarero A, Ambrazevicius G, Cardona M, Schmitz J and Rössler U 1989 *Phys. Rev.* B **39** 13378
[11] Czajkowski G, Bassani F and Silvestri L 2003 *Riv. Nuovo Cimento* **26** 1–150
[12] Kobayashi M, Kanisawa K, Misu A, Nagamune Y, Takeyama S and Miura N 1989 *J. Phys. Soc. Japan.* **58** 1823–30
[13] Artyukhin S, Fishman D, Faugeras C, Potemski M, Revcolevschi A, Mostovoy M and van Loosdrecht P 2018 *Sci. Rep.* **8** 7818
[14] Sobol M and Bardyszewski W 2006 *Phys. Rev.* B **73** 075208
[15] Bardyszewski W and Łepkowski S 2014 *Phys. Rev.* B **90** 075302

[16] Stahl A and Balslev I 1987 *Electrodynamics of the Semiconductor Band Edge* (Berlin: Springer)
[17] Zielińska-Raczyńska S, Czajkowski G and Ziemkiewicz D 2016 *Phys. Rev.* B **93** 075206
[18] Heckötter J, Frölich D, Aßmann M and Bayer M 2018 *Phys. Solid State* **60** 1595
[19] Lamb W E Jr 1952 *Phys. Rev.* **85** 259
[20] Gor'kov L P and Dzyaloshinskii I E 1961 *Sov. Phys. JETP* **26** 449–51
[21] Abramowitz M and Stegun I 1965 *Handbook of Mathematical Functions* (New York: Dover)
[22] Hecktötter J, Freitag M, Frölich D, Aßmann M, Bayer M, Grünwald P, Schöne F, Semkat D, Stolz H and Scheel S 2018 *Phys. Rev. Lett.* **121** 097401
[23] Zielinska-Raczynska S, Czajkowski G, Karpiński K and Ziemkiewicz D 2019 *Phys. Rev.* B **99** 245206
[24] Mott N F and Massey H S W 1965 *The Theory of Atomic Collisions* (*Int. Series of Monographs in Physics*) 3rd edn (Oxford: Oxford University Press)
[25] Czajkowski G, Bassani F and Tredicucci A 1996 *Phys. Rev.* B **54** 2035
[26] Stolz H, Schöne F and Semkat D 2018 *N. J. Phys.* **20** 023019
[27] Gradshteyn I and Ryzhik I 2007 *Table of Integrals, Series, and Products* 7th edn ed A Jeffrey and D Zwillinger (Amsterdam: Elsevier)
[28] Mooser E and Schlüter M 1973 *Il Nuovo Cimento* **18** 164
[29] Aldrich C H, Fooler C M, Caird R S, Garn W B and Witteman W G 1981 *Phys. Rev.* **23** 3970
[30] Baldereschi A and Bassani F 1970 *Proc. 10th Int. Conf. on Semiconductors* ed S P Kellner *et al* (Cambridge, MA: Atomic Energy Comission) p 191